31st Congress of the International Council of the Aeronautical Sciences

Belo Horizonte, Brazil; September 09-14, 2018

HANDLING QUALITIES OF ONERA'S SMALL BUSINESS CONCEPT PLANE WITH DISTRIBUTED ELECTRIC PROPULSION

E. DILLINGER[**,*] , C. DÖLL[*] , R. LIABOEUF[*] , C. TOUSSAINT[*] , J. HERMETZ[*] , C. VERBEKE[*] , M. RIDEL[*]

[*]ONERA – The French Aerospace Lab , [**]ISAE-SUPAERO

Keywords: *distributed electric propulsion, aero-propulsive synergy effects, differential thrust, flight domain, handling qualities*

Abstract

The handling qualities (HQ) of ONERA's small business concept plane AMPERE with Distributed Electric Propulsion (DEP) are assessed. The wind tunnel test data are pre-processed to isolate the aero-propulsive synergy effects. All tabulated coefficients are approximated by polynomials before being included into a flight mechanics model which is trimmed to determine the flight domain and linearized to analyse the eigenvalues. Beyond the HQ-analysis of AMPERE configuration itself, the overall goal is to introduce an HQ-module in a Multidisciplinary Design and Optimization (MDO) tool in order to identify design rules for such DEP configurations and to define and tune innovative control laws using both engines and classical control surfaces for an improved control, especially during critical flight conditions or degraded modes.

Fig. 1 Three-surface concept plane with distributed Electric Ducted Fans EDF at the wing trailing edge

1 Context and Objectives

ONERA–The French Aerospace Lab and CEA (The French Atomic and Alternative Energy Agency) have been running a one year task force in 2012-2013 on the feasibility of electrically powered aircraft. This task force concluded that an electrically powered regional transport aircraft is a conceptually feasible solution when flying slower at lower altitudes with a smaller range and using distributed propulsion [1].

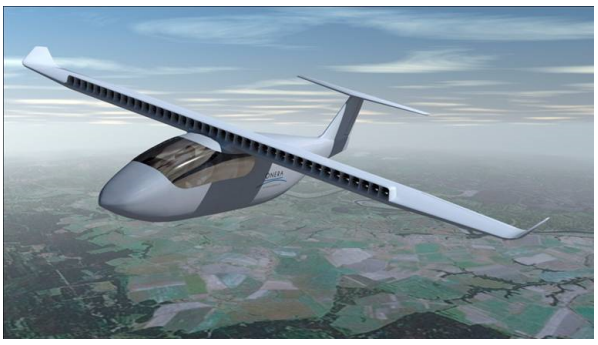

Fig. 2 AMPERE : High-wing concept plane with distributed Electric Ducted Fans EDF along the wing leading edge

In 2014-2015, ONERA has been studying two concept planes [2] in an overall A/C predesign task satisfying the following Top Level Aircraft Requirements TLARs in compliance with CS23 regulations, see Fig. 1 and 2. The small business aircraft for on–demand missions

Characteristics	Symbol	Units	Scale 1	Scale 1:5
Maximum Take-Off Weight (MTOW)	m_{MTOW}	$[kg]$	2400	27
Reference surface	S	$[m^2]$	25.925	1.037
Span	b	m	14.5	2.9
Mean Aerodynamic Chord (MAC)	l	m	1.87	0.373
Payload		PAX	4-6	N/A
Number of engines	n_{eng}	$[-]$	40	32
Installed Energy	E	$[kWh]$	500	external
Installed Power	P	$[kW]$	400	19.2
Horizontal Tailplane (HTP) area	S_{HTP}	$[m^2]$	3.8	0.152
Vertical Tailplane (VTP) area	S_{VTP}	$[m^2]$	2.02	0.081

Table 1 AMPERE's main characteristics

carry 4 to 6 passengers over a range of $500\,km$ in about 2 hours with Short Take-off and Landing STOL capabilities at zero-emission thanks to Distributed Electric Propulsion (DEP) and fuel cells assisted by batteries. The ceiling is under Flight Level FL100 at $10000\,ft$ in order to allow an unpressurized cabin.

ONERA's main objective is to assess the identified key technologies which are :

- DEP using Electric Ducted Fans (EDF)
- Lateral control thanks to the combination of differential thrust with reduced classical control surfaces
- Modular architecture with inflight reconfiguration capabilities of the overall electric propulsion system

and to anticipate major evolutions and disruptive concepts while improving its Multidisciplinary Design and Optimization (MDO) capabilities as well as by taking into account new disciplines, namely thermal aspects and Electro-Magnetic Compatibility (EMC), during the overall design process.

Both planes have a T-tail. The first one (see Fig. 1) is a low wing configuration with a canard. The EDFs are installed at the trailing edge on the suction side of the wing. In addition to a potential slipstream effect, a small Boundary Layer Injection (BLI) impact is expected to reduce drag.

The second one, called AMPERE, see Fig. 2, is a more conventional high-wing configuration with the EDFs installed at the leading edge on the suction side of the wing. The EDFs are then used as an high-lift device for take-off and landing thanks to an aero-propulsive synergy effect called engine-slipstream effect. Its main characteristics are summarized in Tab. 1.

Fig. 3 The AMPERE scaled 1:5 model in ONERA's L2 wind-tunnel

The latter one has been studied in more detail during the AMPERE project, under CARNOT funding, in 2015-2017. 2D and 3D Computational Fluid Dynamics (CFD) in 2015 lead to an optimised design of the EDF integration (location, tilt and local geometry) maximizing the slipstream effect. A scaled 1:5 powered mock-up has then been designed and built in 2016 with 32 slightly bigger COTS EDF with 50mm diameter delivering the same global thrust than 40

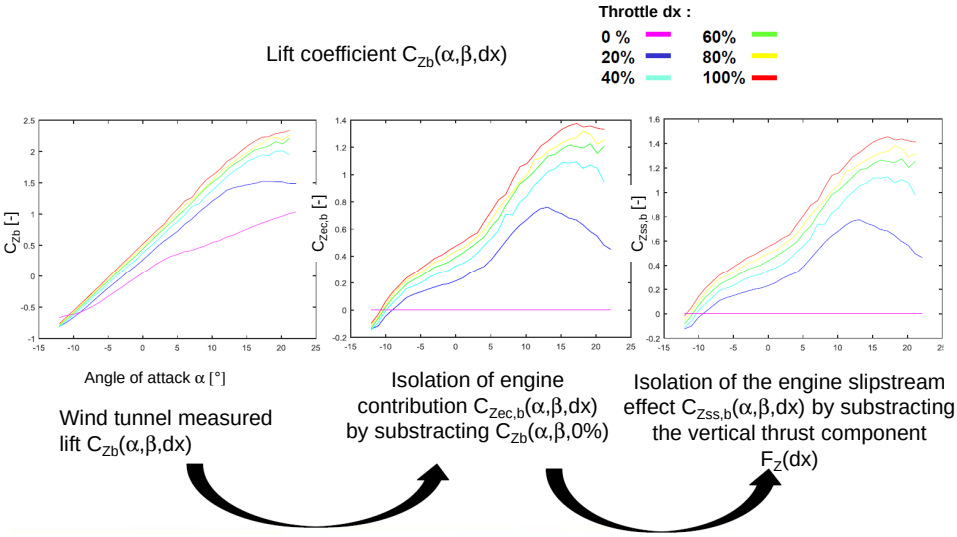

Fig. 4 The isolation of the engine slipstream effect on the lift coefficient in body axis C_{Zb}

EDF with 40mm diameter. Refer to [3, 4] for more details. It has finally been tested in ONERA's low speed wind-tunnel L2 for 4 months end of 2016, beginning of 2017 at $V = 19 m/s$, see Fig. 3 for the installation in the wind-tunnel. 316 different tests have been realized in order to evaluate its aero-propulsive synergy effects in nominal conditions as well as its static performance and dynamic behaviour in off-nominal conditions, *e.g.* at very high angles of attack α and/or high sideslip angles β, and in failure cases, *e.g.* with one, several or all engines inoperative.

2 Evaluation of the engine-slipstream effect

2.1 Nominal conditions

The tests in nominal conditions allowed us to confirm AMPERE's predicted performances exploiting the engine slipstream effect. For example, ONERA's 3D CFD design tools predicted a maximum lift coefficient $C_{Zb,max}$ in body axis of about 3 at an angle of attack α of about 20^o for a clean configuration without high-lift devices. The left plot of C_{Zb} on Fig. 4 proofs a $C_{Zb,max}$ of 2.4 at $\alpha = 22^o$ for full thrust $dx = 100\%$. The curve starts to inflect but not yet to decrease due to stall. This is a typical value which can only be reached using classical high-lift devices, *i.e.* slats and flaps on classical aircraft configurations. Additional wind tunnel tests with another mock-up installation will be realized in the near future to evaluate the stall behaviour beyond $\alpha \geq 22^o$.

Also the lift gradient $C_{Z\alpha,b}$ increases as expected thanks to the slipstream effect in a strong nonlinear way. At zero thrust $dx = 0\%$, $C_{Z\alpha,b}$ is about 2.85. It doubles to 5.7 at a thrust setting of $dx = 40\%$. It further increases to 6.9 at full thrust $dx = 100\%$.

The aero-propulsive synergy effect has to be isolated from the classical aerodynamic forces and moments of the clean aircraft configuration at zero thrust for the flight mechanics modelling. In fact, the isolation enables us to extrapolate the aero-propulsive synergy effect to other flight conditions than the one used in the wind-tunnel, *e.g.* to other speeds V and altitudes h via the air density ρ, and to compare the AMPERE configuration with the slipstream effect to a configuration without aero-propulsive synergy effect. The wing reference surface S allows us to take into account that not the whole wing is exposed to the aero-propulsive synergy effect $S_{aps} < S$, especially in the case of engine failures.

For example, the vertical engine slipstream effect $C_{Zss,b}(\alpha,\beta,dx)$ in body axis is isolated following Fig. 4 in two steps :

1. Substract from the total vertical force $Z = \rho/2V^2SC_{Zb}(\alpha,\beta,dx)$ at throttle setting dx on the left plot the classical aerodynamic lift of the clean aircraft configuration at zero thrust $L = \rho/2V^2SC_{Zb}(\alpha,\beta,0\%)$ in order to isolate the engine contribution $Z_{ec} = \rho/2V^2SC_{Zec,b}(\alpha,\beta,dx)$ to the vertical force which is depicted on the plot in the middle.

2. Substract from this engine contribution $Z_{ec} = \rho/2V^2SC_{Zec,b}(\alpha,\beta,dx)$ the vertical thrust component $F_Z(dx)$ in order to get finally the engine slipstream effect $Z_{ss} = \rho/2V^2SC_{Zss,b}(\alpha,\beta,dx)$ on the right plot.

The engine slipstream effect contributes with $C_{Zss,b}(100\%) = 1.5$ to the global $C_{Zss,b}(100\%) = 2.4$ at $\alpha = 22^o$ whilst the clean aircraft configuration just contributes with $C_{Zb}(0\%) = 0.9$. This positive engine slipstream effect is reduced by the vertical thrust component $F_Z(dx)$ due to the engine installation on the leading edge of the suction side of the wing. $F_Z(dx)$ is in fact oriented downwards and therefore slightly negative. This negative contribution is about -0.1 at $\alpha = 22^o$ as $C_{Zec,b}(100\%) = 1.4$ instead of $C_{Zss,b} = 1.5$.

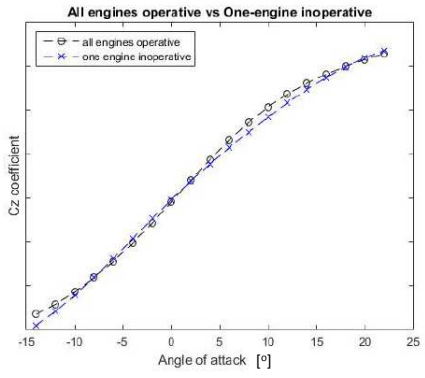

Fig. 5 The comparison between the lift coefficients $C_{Zb}(\alpha)$ for $dx = 50\%$ in nominal and OEI conditions

2.2 One Engine Inoperative (OEI) case

During the wind-tunnel campaign, a series of tests has been conducted with One Engine Inoperative (OEI). The 28^{th} engine[1] has been switched-off in order to evaluate the effect of OEI conditions on the forces and moments. It's the fourth engine from the right wing tip. The tests have been conducted with the fan blocked or in wind-milling conditions.

The comparison between the lift coefficients $C_{Zb}(\alpha)$ in nominal and OEI conditions is for example shown on Fig. 5 for a thrust setting of $dx = 50\%$. As expected, there is a small effect at medium angle of attacks α, corresponding to the $\frac{1}{32}C_{Zss,b}$, which is neglectible with respect to the remaining $\frac{31}{32}C_{Zss,b}$. The slipstream effect can therefore be exploited even in the case of several engine failures.

3 The propulsion module

The thrust has also been adimensionalized with respect to ρ, V and S. The resulting coefficient

$$C_F = \frac{F(\rho,V,dx)}{\frac{\rho}{2}V^2S} \tag{1}$$

is called thrust coefficient.

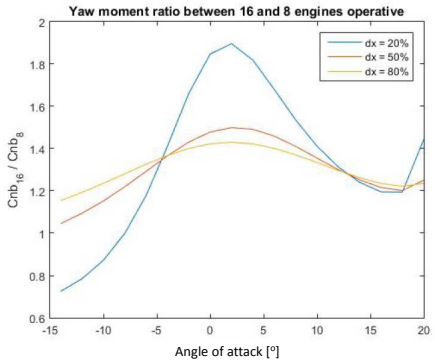

Fig. 6 The ratio between the yaw coefficients $C_{nb,16}/C_{nb,8}(\alpha)$ for different thrust settings with 16 or 8 right engines operative

[1] Engine within the wing section on which some pressure taps are located in order to analyse local pressure distortion.

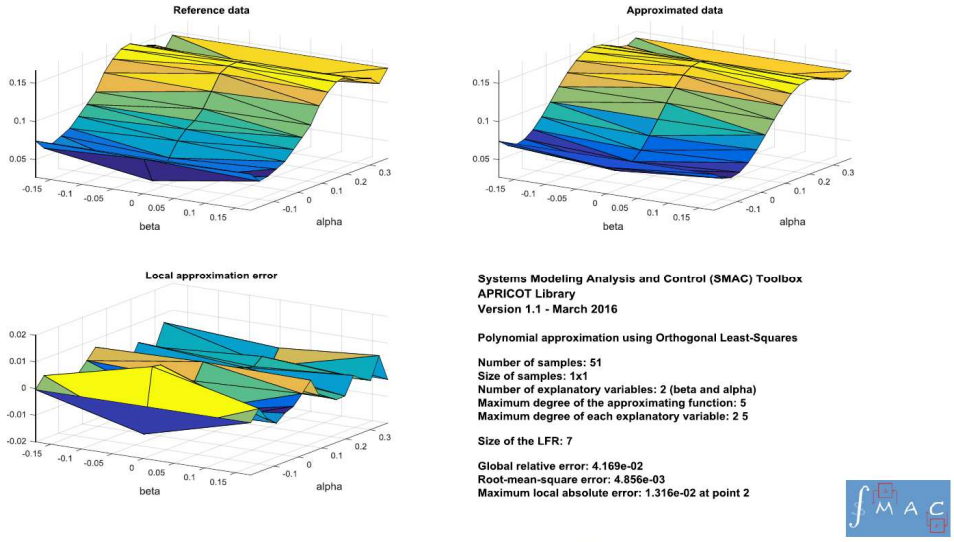

Fig. 7 Comparison between the drag coefficient $C_{X0}(\alpha,\beta)$ measured during the wind-tunnel tests and the one obtained by polynomial approximation using the APRICOT Library of ONERA's SMAC toolbox for use with Matlab©

The creation of yaw and roll moment thanks to the differential use of the 32 engines has been evaluated during several series of wind-tunnel tests. For that purpose, all 16 engines on the left wing have been switched-off. For a first series of tests, all 16 engines on the right wing have been set to the same thrust setting dx. For a second series of tests, just the 8 outer engines on the right wing have been used. For example, Fig. 6 shows the ratio $C_{nb,16}/C_{nb,8}$ between the created yaw moment coefficients using the 16 and 8 right engines. Obviously, it is more efficient to use all 16 engines than just the 8 outer ones. However, the ratio depends on the thrust setting : Whilst for $dx = 20\%$, the ratio is almost 2 as expected, it is more or less constant and about 1.4 for $dx \geq 50\%$. This is due to the fact, that the efficiency of the engines to create yaw and roll decreases with the thrust setting and that the outer engines have a bigger lever arm with respect to the centre of gravity than the inner engines. The use of the engines for yaw control is therefore particularly interesting at low thrust settings, which correspond to low speed settings.

4 Approximation of the aerodynamic coefficients

All aerodynamic coefficients obtained directly by the wind-tunnel tests or after the pre-treatment from §2 are tabulated with respect to the angle of attack α, the sideslip angle β and/or the throttle level dx. In order to simplify the trimming and linearization steps necessary for the handling quality assessment, all coefficients are approximated by polynomial expressions using the APRICOT orthogonal least-squares algorithm of ONERA's System Modelling, Analysis and Control Toolbox [5] for use with Matlab©. The user chooses just the highest degrees of the explanatory variables α, β and dx in the polynomial and a maximum error (either global, local or root-mean-square, absolute or relative). Thanks to the orthogonal decomposition, the algorithm retains then just the monomials which reduce significantly the error between the polynomial approximation and the original data. The result of such a polynomial approximation is illustrated on Fig. 7 for the drag coefficient $C_{X0}(\alpha,\beta)$. On the left upper side, the original wind tunnel data for

$C_{X0}(\alpha,\beta)$ are plotted. For the explanatory variables, α with a maximum degree of 5 and β with a maximum degree of 2 have been chosen. The polynomial

$$C_{X0}(\alpha,\beta) = c_0 + c_1\,\alpha + c_2\,\alpha^3 + c_3\,\alpha^5 + c_4\,\alpha\beta$$

produces the plot on the right upper side. The local absolute approximation errors are plotted on the left lower side, its maximum is 0.0132 for the second data point, the global relative error is about 4%.

5 Flight Mechanics Model

The rigid body mechanics are expressed in the aircraft body frame (x_b, y_b, z_b) in order to obtain the flight dynamics equations. For more details on the definition of the different reference frames, see for example the lecture notes [6]. The rotations from the earth reference frame into the body frame introduce the bank angle ϕ, the pitch angle θ and the heading angle ψ. The rotation rates are given by the roll rate p, the pitch rate q and the yaw rate r.

The aircraft is supposed to be symetric with respect to the plane (x_b, z_b), therefore the inertia matrix J becomes :

$$J = \begin{pmatrix} A & 0 & -E \\ 0 & B & 0 \\ -E & 0 & C \end{pmatrix} \tag{2}$$

Neglecting time variations in mass and inertia, the designer gets the following 9 differential equations :

$$\begin{aligned}
\dot{v}_X &= \frac{\Sigma F_{X\,ext}}{m} - q\,v_Z + r\,v_Y - g\sin\theta \\
\dot{v}_Y &= \frac{\Sigma F_{Y\,ext}}{m} - r\,v_X + p\,v_Z + g\cos\theta\sin\phi \\
\dot{v}_Z &= \frac{\Sigma F_{Z\,ext}}{m} - p\,v_Y + q\,v_X + g\cos\theta\cos\phi \\
A\dot{p} - E\dot{r} &= \Sigma M_{X\,ext} + (B-C)\,qr + Eqp \\
B\dot{q} &= \Sigma M_{Y\,ext} + (C-A)\,rp - E(p^2 - r^2) \\
C\dot{r} - E\dot{p} &= \Sigma M_{Z\,ext} + (A-B)\,pq - Eqr \\
\dot{\phi} &= p + \tan\theta\,(r\cos\phi + q\sin\phi) \\
\dot{\theta} &= q\cos\phi - r\sin\phi \\
\dot{h} &= v_X\sin\theta - v_Y\cos\theta\sin\phi - v_Z\cos\theta\cos\phi
\end{aligned} \tag{3}$$

The external forces $\vec{F}_{ext}$ and momentum $\vec{M}_{ext}$ on the aircraft are stemming from :

- classical aerodynamic efforts $(\vec{F}_{aero}, \vec{M}_{aero})$,
- classical propulsion efforts $(\vec{F}_{mot}, \vec{M}_{mot})$
- and the new aero-propulsive synergy effects depending on the engine installation and the aircraft configuration, here the slipstream effects $(\vec{F}_{ss}, \vec{M}_{ss})$.

The speed vector (v_X, v_Y, v_Z) is replaced by (V, α, β), where V is the speed module or airspeed, α the angle of attack and β the sideslip angle :

$$\begin{aligned}
v_X &= V\cos\alpha\cos\beta \\
v_Y &= V\sin\beta \\
v_Z &= V\sin\alpha\cos\beta
\end{aligned} \tag{4}$$

Eq. (3) corresponds to the nonlinear system :

$$\begin{aligned}
\dot{x} &= f(x,u) \\
y &= g(x,u)
\end{aligned} \tag{5}$$

where the state vector x becomes finally $(V, \alpha, \beta, p, q, r, \phi, \theta, h)^T$. The inputs u are the n_{eng} thrust settings dx_i in addition to the classical aileron, elevator and rudder deflections $(\delta l_i, \delta m_i, \delta n_i)^T$. The model outputs y contain the states x and the load factors calculated as follows:

$$\begin{aligned}
n_X &= \frac{\Sigma F_{X\,ext}}{mg} \\
n_Y &= \frac{\Sigma F_{Y\,ext}}{mg} \\
n_Z &= -\frac{\Sigma F_{Z\,ext}}{mg}
\end{aligned} \tag{6}$$

By convention, the vertical load factor is positive downwards.

Based on the aerodynamic coefficients from §4, the propulsion module from §3, the aero-propulsive synergy effect isolated in §2, the mock-up's geometry and inertia data from Tab. 1 and a classical International Standard Atmosphere ISA model, the flight mechanics model can be built.

For that purpose, a modular solution based on Matlab© objects has been coded. A `Model` object is created for AMPERE. This object has a list of `Force` objects. One `Force` object corresponds to the representation of one physical phenomenon (gravity, aerodynamics, ...). A new `Force` can be added to the model in order to take into account a certain aero-propulsive synergy effect or the landing gear force for instance or removed easily. The `Force` class defines a `compute` method which executes the force modelling and a `get` method which enables to express a force in a given frame and moments at a given point. Based on that, `model.newton(x)` will compute vehicle dynamics using `x` as state vector. Several `Criterion` objects are defined in order to assess vehicle handling qualities in various flight conditions. These criteria use equilibrium solvers, linearizers and dynamic simulators. The `Criterion run` method will return a value representing how well the defined criterion is satisfied.

6 Flight domain assessment

All results described in the following sections are based on the scaled AMPERE mock-up. Their transposition to the original scale shall be realized in a future project's phase.

6.1 Trimming procedure

The designer is interested in all flight conditions where the pilot manages to stabilize the aircraft in a steady state. For example, the main flight conditions of interest are level flight in cruise, a constant climb or descent, take-off or landing with cross-wind, a constant turn with or without sideslip angle. These steady states are also called equilibrium states or trim conditions. The flight domain of an aircraft is determined by the attainable flight conditions (mass, centre of gravity position, speed, altitude) where at least one of the control surfaces and/or engines is at its limits.

Equilibrium states are therefore computed by fixing a certain number of magnitudes :

- h
- V or the elevator deflection δm_i of each elevator
- v_Z or the thrust setting dx_i of each engine
- two magnitudes amongst ϕ, β, r and the rudder deflection δn_i of each rudder

Starting with Eq. (5), the equilibrium computation consists in finding x_{eq} and u_{eq} satisfying the above constraints such that $f(x_{eq},u_{eq}) = 0$ except of the equation for h where $\dot{h} = -v_Z$. In the general case, this problem is an optimization problem under constraints.

The solution of an optimization problem under constraints has been coded in order to be able to treat all imaginable trim conditions in a generic and modular way. This solver is used by providing a set of free parameters (the ones the solver will change), a set of constrained parameters, the constraints targets (for instance all derivatives equals to 0) and an objective function.

For example for the AMPERE configuration using distributed propulsion, the following constrained optimization problem can be solved:

$$\begin{array}{lll} \min\limits_{(x,u)} & \sum_{i=1}^{n_{eng}} & N\left(\delta x_i - \delta\bar{x}\right) \\ \text{uc}\ \dot{x} & = & f(x_{eq},u_{eq}) = 0 \end{array} \tag{7}$$

which will find an equilibrium point that minimizes the thrust variation from average thrust $\delta\bar{x}$ for a given norm N at a given flight point (i.e. some elements of x_{eq} and u_{eq} are given).

6.2 Flight Domain

The AMPERE configuration exploiting the slipstream effect (5) is first trimmed at various flight conditions in speed and altitude (V,h) for several centre of gravity positions X_{CG} in level flight using Eq. (7) in order to determine its longitudinal flight domain, which is given on Fig. 8. See Fig. 9 for the corresponding elevator deflections δm, angles of attack α and thrust levels dx in trimmed level flight for $h = 0\,m$ and $X_{CG} = 0.8\,m$.

As expected, the flight domain is limited at high speeds by the throttle setting with $dx =$

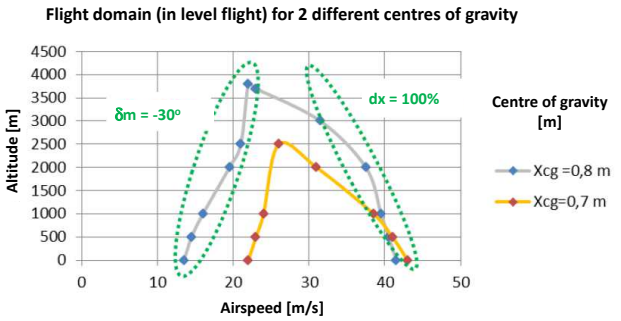

Fig. 8 The flight domain in level flight of the AMPERE mock-up for two different X_{CG}-positions exploiting the slipstream effect at low speeds

100%. The corresponding elevator deflections and angle of attacks are small, for instance at $X_{CG} = 0.8\,m$, $h = 0\,m$, $V = 40\,m/s$, the elevator deflection is $\delta m = 2.2^o$ with an angle of attack $\alpha = 1.8^o$. At low speeds, it is limited by the maximum elevator deflection $\delta m = -30^o$. The corresponding thrust settings at low speeds are small, for instance at $X_{CG} = 0.8\,m$, $h = 0\,m$, $V = 14\,m/s$, dx reaches just 25% at a reasonable angle of attack $\alpha = 13.6^o$, which means that the pilot is able to slow down in clean configuration by exploiting the slipstream effect without having to increase significantly the thrust setting. He does neither not need to deflect any airbrakes.

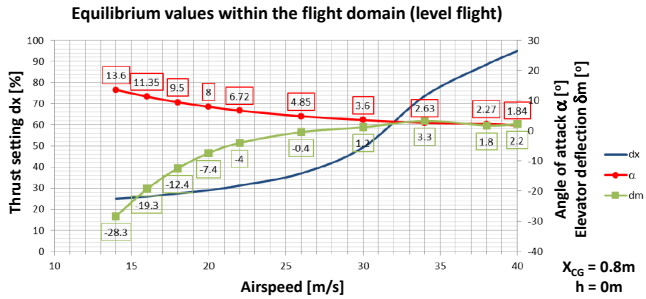

Fig. 9 δm, α and dx for trimmed level flight of the AMPERE mock-up in function of V at $X_{CG} = 0.8\,m$ and $h = 0\,m$

Thanks to the slipstream effect, the low speed limit allows to take–off in a short distance in clean configuration, which was one of the TLARs. The landing speed in clean configuration could however be further reduced by either increasing the elevator efficiency C_{mdm} and/or by increasing the elevator surface S_{el} and/or by using a trimable HTP without a significant thrust increase. For more details on the flight domain extension using a trimable HTP refer to [7]. In the same reference, the flight domain of AMPERE in terms of (X_{CG}, V) has extensively been analysed and the AMPERE configuration has been compared to an AMPERE like configuration without slipstream effect using a classical high lift device for low speed.

Another advantage of the Distributed Electric Propulsion (DEP) is the possibility to trim the aircraft both longitudinally as well as laterally in the case of some engine failures not only by the rudder and aileron deflection but also using the remaining engines. For example, with AMPERE it is possible to counter the failure of the 8 outer left engines in level flight by switching-off the 2 outer right engines and by setting the remaining 22 engines at $dx = 65\%$ with a rudder deflection $\delta n = -28.2^o$, an aileron deflection $\delta l = -4^o$ and an elevator deflection $\delta m = 14.8^o$ while keeping the wing in an horizontal position at $\phi = 0^o$ with $\alpha = 4.6^o$ and $\beta = -3.4^o$ at $h = 200\,m$, $V = 25\,m/s$ and $X_{CG} = 0.8\,m$. Without differential thrust, the rudder deflection would have been saturated. For more details on the impact of the differential thrust on the lateral equilibriums, especially on the minimum control speed V_{MC} and the rudder sizing for similar aircraft configurations with or without slipstream effect, see [8, 9].

7 Handling Qualities assessment

The nonlinear system (5) is linearized around various flight conditions, *i.e.* equilibrium states $\dot{x} = 0$ or pseudo-equilibriums $\dot{h} = -v_Z = \text{constant}$ in order to obtain the linear state space representations

$$\begin{aligned} \dot{x} &= Ax + Bu \\ y &= Cx + Du \end{aligned} \tag{8}$$

The eigenvalues of the dynamics matrix A are plotted on Fig. 10. As expected, the phugoid of

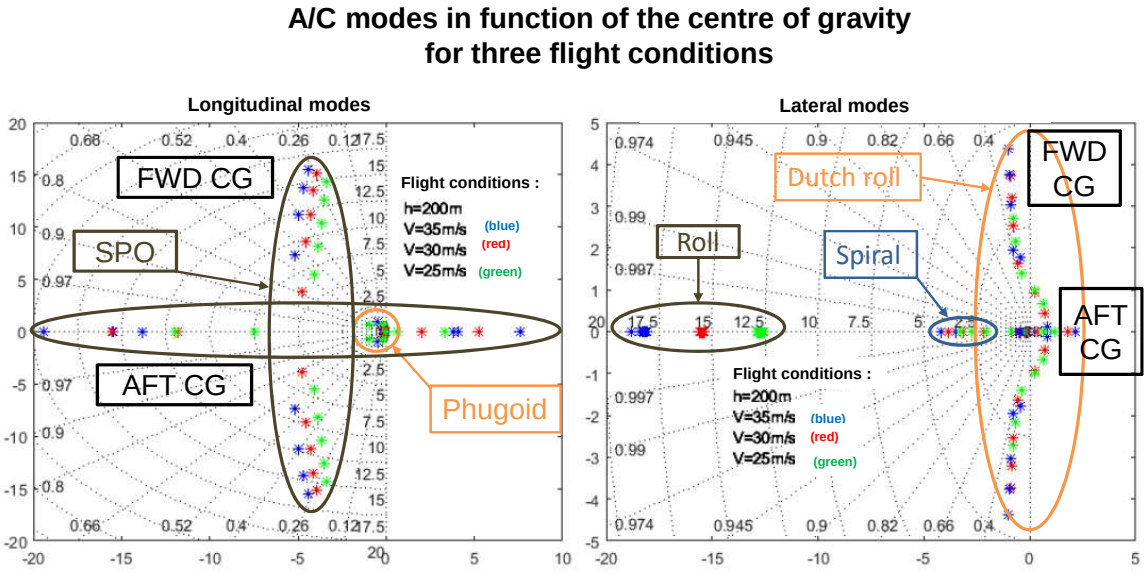

Fig. 10 The modes of the AMPERE mock-up in function of the X_{CG}-position at three different flight conditions

the mock-up is a quite slow, badly damped oscillatory mode which does not depend on the centre of gravity position X_{CG}. It does only depend on the airspeed V.

The short period oscillation mode (SPO) also depends on the airspeed V, but the SPO mainly depends on the X_{CG} position as on classical aircraft. When shifting X_{CG} aftwards, the SPO's complex conjugated poles first get closer to the real axis with the same real part, before becoming two real poles. One of them is then shifting to the right, reaching the origin of the complex plane when the centre of gravity reaches the mean aerodynamic centre $X_{CG} = X_{NP}$ and even becoming unstable when X_{CG} is behind X_{NP}. The divergence of the angle of attack is a pure exponential function, which can be easily countered by the pilot as long as the time to double is less than 6 seconds. The SPO is faster than on classical aircraft and moderately damped. This is due to the small scale of the mock-up.

The roll and spiral mode are both aperiodic and fast modes which do not depend on X_{CG}. They just depend on V. The roll mode is as usually much faster than the spiral one, but they are both much faster than for a classical aircraft. This is due to the small scale of the mock-up on the one hand and to a big aileron efficiency C_{ldl} on the other. The dutch roll mode depends as expected on X_{CG}, it is very badly damped and faster than on classical aircraft. This is due to the small scale of the mock-up on the one hand and a small rudder efficiency C_{ndn} on the other hand. For aft X_{CG} positions, the dutch roll becomes unstable as on a classical aircraft. In contrast to the SPO, the instability is however an oscillating one, which increases the workload of the pilot to counter the divergence. There is a risk of Aircraft Pilot Coupling (APC).

8 Conclusions and Perspectives

Based on this model, flight control laws are synthesized at the moment in order to improve the natural handling qualities and to exploit the possibility to create yaw by using differential thrust with the DEP whilst not increasing the pilot's workload by optimal control allocation schemes. The differential thrust will allow to reduce the vertical tail and the rudder. The possible size reduction will be determined in terms of handling qualities in nominal and failure conditions. The outcomes shall contribute to improve the initial design of the AMPERE concept-plane and to highlight the whole potential of DEP for light air-

craft. The HQ-module including the flight control laws design tool will be integrated into the MDO process in order to optimize all kind of new aircraft configurations using DEP.

References

[1] C. Döll, B. Paluch, A. Guigon, and D. Fraboulet. Conceptual feasibility study for a fully electrically powered regional transport aircraft. In *Proc. 29th ICAS Congress*, St. Petersburg, Russia, September 2014. http://publications.onera.fr/exl-php/docs/ILS_DOC/281623/DOC414926_s1.pdf

[2] J. Hermetz. L'avion d'affaire personnel à propulsion électrique, un concept-plane? In *Aéro-Club de France*, Paris, France, April 2014. http://www.onera.fr/sites/default/files/Departements-scientifiques/DCPS/ONERA-Aero-Club-de-France.pdf

[3] J. Hermetz, M. Ridel, and C. Döll. Distributed electric propulsion for small business aircraft — a concept-plane for key-technologies investigations. In *Proc. 30th ICAS Congress*, Daejeon, South Korea, September 2016.

[4] J. Hermetz, L. Guibert, M. Ridel, and D. Gonzales-Condé. Distributed electric propulsion for small business aircraft. In *Proc. More Electric Aircraft MEA*, Bordeaux, France, February 2017.

[5] J.M. Biannic. *Systems Modeling, Analysis and Control Toolbox*. http://w3.onera.fr/smac/, 1st edition, June 2016.

[6] J.L. Boiffier. *The dynamics of flight : The equations*. John Wiley & Sons, August 1998.

[7] R. Liaboeuf and E. Dillinger. Onera's small business concept plane with Distributed Electric Propulsion longitudinal Handling Qualities evaluation. In *Proc. 18th ONERA-DLR Aerospace Symposium ODAS*, Bonn, Germany, July 2018.

[8] E. Nguyen Van. Towards an aircraft with reduced lateral static stability using Electric Differential Thrust. In *Proc. AIAA Aviation Forum*, Atlanta, Georgia, USA, June 2018.

[9] E. Nguyen Van. Influence of differential thrust with Distributed Electric Propulsion on lateral static stability. In *Proc. 18th ONERA-DLR Aerospace Symposium ODAS*, Bonn, Germany, July 2018.

Acknowledgements

The authors are grateful for the funding provided by the CARNOT Label 11 CARN 034-01 http://www.instituts-carnot.eu/.

The authors would like to thank ISAE-SUPAERO and CEDAR (Chair for Eco Design of AircRaft), sponsored by AIRBUS, for their financial support to the first author's travel expenses. The authors would also like to thank all their colleagues from ONERA who have contributed to the overall project, and especially O. Atinault, M. Lamoureux (Aerodynamics, Aeroelasticity and Acoustics Depart.), B. Paluch (Materials and Structures Depart.), Ph. Choy, F. Demourant, A. Janot and P. Schmollgruber (Information Processing and Systems Depart.), D. Donjat (Multi-Physics and Energetics Depart.), L. Guibert (Electromagnetics and Radar Depart.) and last but not least A. Guigon (Prospective Depart.).

Contact Author Email Address

For more details, you can contact:
Carsten.Doll@onera.fr
Romain.Liaboeuf@onera.fr

Copyright Statement